Quantum-Chemical Study of the Adsorption of DMMP and Sarin on γ-Al_2O_3

V. M. Bermudez†

Electronics Science and Technology Division, Naval Research Laboratory, Washington, DC 20375-5347

Received: October 1, 2006; In Final Form: November 27, 2006

Ab initio calculations, using density functional theory with the B3LYP functional, have been applied to the adsorption of the chemical warfare agent simulant dimethyl methylphosphonate (DMMP) and the corresponding real agent Sarin on γ-Al_2O_3. The goals are to determine the accuracy with which the adsorbed molecules (for which experimental data are available) can be modeled and to conduct a "side-by-side" comparison of the bonding of these species to γ-Al_2O_3. Free-standing Al_8O_{12} and $Al_{20}O_{30}$ clusters give reasonable descriptions of the adsorbate structure and properties, and the results are not strongly dependent on cluster size or basis-set quality. For either molecule, the energetically favorable mode of adsorption is Al−O═P dative-bond formation, in agreement with experiment. Results for the physisorption of H_2O are compared to those reported for a two-dimensionally periodic slab in order to test the reliability of the free-standing cluster model. The adsorption energy of DMMP on the $Al_{20}O_{30}$ cluster (−57.5 kcal/mol at the 6-311G(df) level) is greater than that of Sarin (−49.2 kcal/mol). The infrared-active normal-mode frequencies for free DMMP and Sarin have been used to verify the reported mode assignments for these species. For the adsorbed molecules, the ν(P═O) stretch shows a red-shift (relative to the gas phase) of ∼60 cm^{-1} (observed) vs about 84 cm^{-1} (calculated). The calculated shifts for other modes are much smaller and generally agree with experiment.

1. Introduction

The interaction of chemical warfare agents (CWAs) with materials is an issue of immediate practical concern. Real CWAs are far too dangerous for experimental study at any but a small number of specially equipped facilities, which limits the rate at which such compounds can be investigated and characterized. Hence, most exploratory work on CWA detection and remediation is done using simulants, i.e., species which are safe enough for routine handling and which (it is hoped) behave in a manner closely similar to real CWAs. It is problematic to compare directly the simulant and the corresponding CWA, again because of the difficulties inherent in working with the latter. Thus, it is often not possible to evaluate the degree to which the simulant mimics the real CWA in a particular type of measurement. Ab initio quantum-chemical (QC) theory can, in principle, relieve much of the burden of working with real CWAs through the application of modeling, and several pioneering QC studies of the adsorption and reactivity of CWAs have been reported.[1−9]

The focus of the present work is on the adsorption of a CWA and a simulant on an oxide. We wish to test the reliability of QC methods in this context by comparing calculated results with experimental data and to compare the adsorption behavior of the simulant with that of the real agent. Such a "side-by-side" comparison has not, to our knowledge, been reported in previous theoretical work. The simulant chosen is dimethyl methylphosphonate (DMMP), and the corresponding real agent is the G-series nerve agent Sarin (GB). The relevant molecular structures are shown in Figure 1. The adsorption of DMMP on several materials has been studied experimentally, and γ-Al_2O_3 has been chosen as a representative oxide substrate. γ-Al_2O_3 is of interest in its own right either as a solid adsorbent[10] for air purification or as a catalyst support[11] in the chemical destruction of CWAs. Also, several common materials involve alumina or aluminosilicates. Experimental data (see below) are available for DMMP and Sarin both free and adsorbed on γ-Al_2O_3, which makes the present choice of reagents and substrate particularly useful.

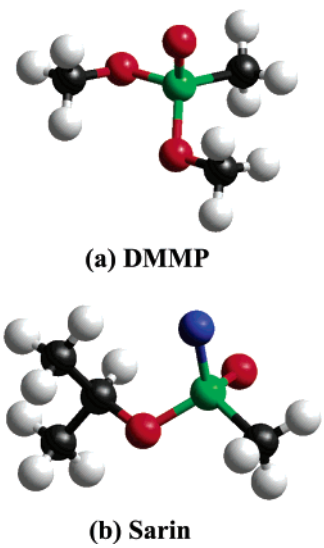

Figure 1. Molecular structures of (a) DMMP and (b) Sarin. Red, green, and blue spheres indicate O, P, and F respectively.

2. Results and Discussion

2.1. The Free Molecules. Unless otherwise noted, all calculations were done using the *Gaussian 03* suite of programs[12] with basis sets built into the package. Both restricted Hartree−Fock (RHF) and density functional theory (DFT) were

† To whom correspondence should be addressed. E-mail: Victor.bermudez@nrl.navy. mil. Phone: +1-202-767-6728. Fax: +1-202-767-1165.

10.1021/jp066439g CCC: $37.00 © 2007 American Chemical Society
Published on Web 02/09/2007

TABLE 1: Observed and Calculated Rotational Constants (MHz) for DMMP

method[a]	A	B	C	Σ|error|[b]
experiment (ref 13)	2828.753	1972.359	1614.268	0
B3LYP/6-31G*	2679.49	1947.53	1579.51	0.087
B3LYP/6-311^{++}G**	2689.79	1933.40	1566.00	0.099
MP2/6-31G*	2714.42	1957.63	1600.25	0.057
MP2/6-311^{++}G** [c]	2744.09	1959.76	1600.47	0.045

[a] The geometry was optimized for each method before computing the rotational constants. The calculated results are for the most stable conformer which is the same for all four methods and which concurs with that given in ref 13. [b] The error is defined as |calc.- obs.|/obs. summed over all three rotational constants. [c] These values are lower by 8−12 MHz than the MP2/6-311^{++}G** results given in ref 13.

TABLE 2: Observed and Calculated Rotational Constants (MHz) for Sarin[a]

method	A	B	C	Σ|error|
experiment (ref 18)	2874.0710	1168.5776	1056.3363	0
B3LYP/6-31G*	2770.95	1136.10	1032.19	0.087
B3LYP/6-311G(df)	2797.31	1138.93	1034.71	0.073

[a] See footnotes a and b in Table 1.

used where appropriate. Further details will be provided as needed in the following discussion.

Since much of the present work focuses on the infrared (IR) vibrational spectra of adsorbed DMMP and Sarin, the first task is to show that the properties of the free molecules can be correctly described. One concern lies in determining the influence of the method of calculation and the choice of basis sets on the accuracy of the final results. To this end, two different methods for dealing with electron correlation are considered, namely, second-order Møller-Plesset (MP2) correction to the RHF wavefunction and DFT with the hybrid B3LYP functional. Basis sets of different quality are also evaluated. The experimentally observable properties of interest are the geometry (i.e., bond lengths and angles) or the rotational constants (which are closely related to the geometry) and the vibrational spectra. It is noted that the P atom is an optically active center in Sarin but not in DMMP. Only one enantiomer (that shown in Figure 1b) is considered here. Optical isomerization is not expected to affect adsorption on an oxide surface but could, conceivably, be of significance in bioactivity.

Previous theoretical studies of DMMP have focused on the conformation in the gas[13] or liquid[14] phase or in aqueous solution[15] and on the IR spectrum of the H-bonded complex[16] with H_2O. Rotational constants derived from microwave spectra[13] are the only available data related to molecular geometry. The results for the rotational constants in Table 1 indicate an average error of about 3% for DFT/B3LYP vs <2% for RHF/MP2. However, there appears to be little dependence on the quality of the basis set. In all cases, the molecule was placed in the lowest-energy conformation (Figure 1a), as identified in ref 13, prior to final geometry optimization.

Previous theoretical studies of Sarin have focused on the conformation in the gas phase.[17,18] The adsorption of Sarin on MgO[3] and on clay[4,9] and its interaction with various reagents[1,2,5,6] have also been investigated using QC methods. Rotational constants are available[18] for Sarin, and these are shown in Table 2 together with results of the present work obtained using DFT with the B3LYP functional and either 6-31G* or 6-311G(df) basis sets. The molecule was initially placed into one of the two nearly degenerate lowest-energy configurations[17,18] prior to optimization. Again, the computed results show very little basis set dependence, although ref 18 indicates that RHF/MP2 gives somewhat better agreement with experiment than does DFT/B3LYP, as was also seen for DMMP (cf. Table 1). In the absolute lowest-energy configuration,[17,18] which lies ∼0.1 kcal/mol below that in Figure 1b, the isopropyl group is rotated ∼90° clockwise about the C−O bond relative to the geometry shown in Figure 1b. However, upon adsorption (see below), this would bring one of the isopropyl $-CH_3$ groups somewhat close to the surface, thus raising the possibility of steric hindrance. Hence, the Sarin configuration shown in Figure 1b was adopted as the starting structure.

The scaling of normal-mode frequencies in ab initio calculations has been discussed extensively. In the present work, B3LYP/6-31G* values were scaled by a factor of 0.9613 (ref 19) and B3LYP/6-311^{++}G** values by a factor of 0.9679 (ref 20). The MP2/6-31G* and 6-311^{++}G** values were scaled by factors of 0.9427 and 0.9496 respectively (ref 21). The uncertainty in these factors[22] is in the range of ±0.020 to ±0.025.

The IR spectra of liquid[23−25] and gas-phase[24−26] DMMP have been reported, and Table 3 compares the observed and calculated frequencies for the mid-IR-active fundamentals. Several footnotes are given in Table 3 and in other tables in order to clarify the correlation between observed and calculated frequencies. This correlation is, in many cases, not obvious without a careful inspection of the results. Comparison is made with gas-phase rather than liquid data since some modes are significantly affected by intermolecular interaction which is not included in the calculation. The average error in the B3LYP/6-31G* results, excluding the $\nu(O-CH_3)$ modes (see below), is about 1.9% in magnitude and does not change significantly for other methods and basis sets. For example, the MP2/6-311^{++}G** average error is about 2.3%. Attention is focused on the IR rather than on the Raman spectrum since the available vibrational data for adsorbed DMMP are in the form of IR spectra. Meaningful comparison cannot be made between observed and calculated $\nu(O-CH_3)$ modes because of Fermi resonance[27] with the δ-$(O-CH_3)$ overtones. This is not included in the calculations, which do not explicitly consider anharmonicity or the excitation of more than one vibrational quantum. A similar consideration does not apply to the $\nu(P-CH_3)$ modes which are well-separated in energy from the $\delta(P-CH_3)$ overtones.

Figure 2 shows calculated (B3LYP/6-31G*) and observed[28] IR absorbance spectra for gas-phase DMMP, mainly for the purpose of comparing the relative intensities. The spectrum was simulated by placing a Gaussian line shape function at each normal-mode energy, with the peak area set equal to the calculated oscillator strength. An arbitrarily chosen full-width at half-maximum of 20 cm^{-1} was assigned to each peak to represent the combined effects of instrumental and rotational broadenings. The spectrum was then obtained by summing all of the individual peaks thus defined. The agreement is seen to be fairly good except for the $\nu(O-CH_3)$ modes, which are affected by Fermi resonance as noted above. However, the "skeletal" modes (e.g., the P═O, P−O and C−O stretches), which are most useful in adsorbate structural assignments, are well represented in the calculated spectrum.

Table 4 compares the observed[29] and calculated fundamental frequencies for Sarin. In this case, only data for the liquid are available, and it is assumed that some modes are affected by intermolecular interaction as was seen for DMMP (Table 3). Hence, direct comparison with the calculated (gas-phase) frequencies is not possible, and error values are not given. The comments made above regarding the Fermi resonance between the $\nu(CH_3)$ fundamentals and the $\delta(CH_3)$ overtones also apply

TABLE 3: Observed and Calculated Mid-IR-Active Fundamental Frequencies (cm^{-1}) for DMMP

mode[a]	obs. (liq.)[b]	obs. (gas)[c]	calc. (gas)[d]	|error|[e]
$\nu_a(P-CH_3)$[f]	2992	3014	3042	0.0093
$\nu_a(O-CH_3)$[g]	2957	2962	3028	0.0223
$\nu_s(P-CH_3)$	2926	2921	2958	0.0127
$\nu_s(O-CH_3)$[h]	2852	2859	2940	0.0283
$\delta_a(O-CH_3)$[i]	1465	1471	1475	0.0027
$\delta_s(O-CH_3)$[j]	1450		1438−1431	
$\delta_a(P-CH_3)$[j]	1419	1423	1438−1431	
$\delta_s(P-CH_3)$	1317	1315	1320	0.0038
$\nu(P{=}O)$	1242	1276	1225	0.0400
$\rho_{\|\|}(O-CH_3)$[k]	1186	1188	1163	0.0210
$\nu(C-O)$[l]	1058	1075	1053	0.0205
$\nu(C-O)$[l]	1034	1050	1030	0.0190
$\rho_{\|\|}(P-CH_3)$[m]	896	919	911	0.0087
$\nu(P-O)$[l,n]	822	818	777	0.0501
$\nu(P-O)$[l]	789		753	
$\nu(P-C)$	714		667	
$\omega(PO_2)$	500		466	

[a] Mode assignments are from ref 23 for liquid DMMP, except where noted. Only mid-IR-active (500−4000 cm^{-1}) modes are included. ν = stretching; δ,ω = deformations; ρ = rocking; s = symmetric; a = asymmetric. [b] Frequencies from ref 23. These are consistent with liquid-phase values given in ref 24. [c] Frequencies from ref 24, except where noted. These are consistent with gas-phase values given in ref 26. [d] B3LYP/6-31G* results after scaling by a factor of 0.9613 (see text). [e] Errors are defined as |calc.- obs.|/obs. where "obs." are gas-phase values. For completeness, error values are also given for the $\nu(O-CH_3)$ modes, but these are affected by Fermi resonance with the $\delta(O-CH_3)$ overtones (see text) which is not included in the calculation. The average error, excluding the $\nu(O-CH_3)$ modes, is 0.019 (i.e., 1.9%) in magnitude. [f] The calculated value is the average of in-plane and out-of-plane modes separated by about 8 cm^{-1}. [g] The calculated value is an average of in-phase and out-of-phase linear combinations of in-plane and out-of-plane modes spread over a range of 33 cm^{-1}. [h] The calculated value is an average of in-phase and out-of-phase linear combinations separated by about 8 cm^{-1}. [i] Reference 24 assigns this mode to $\delta_a(P-CH_3)$, but the calculation supports the assignment given in ref 23. The calculated value is an average of mode energies spread over about 12 cm^{-1}. [j] The calculation indicates that $\delta_a(P-CH_3)$ is strongly mixed with the in-phase and out-of-phase linear combinations of $\delta_s(O-CH_3)$, all of which fall within the range given. Reference 23 assigns the 1419 cm^{-1} liquid mode to $\delta_s'(P-CH_3)$. This assignment has been changed in the Table. [k] The corresponding $\rho_\perp$ mode, calculated to lie at 1142 cm^{-1} in the gas phase, has a calculated intensity equal to ∼5% of that of the $\rho_{||}$ mode. [l] The higher- (lower-) energy mode is the in-phase (out-of-phase) linear combination. [m] The corresponding $\rho_\perp$ mode, calculated to lie at 895 cm^{-1} in the gas phase, has a calculated intensity equal to ∼27% of that of the $\rho_{||}$ mode. [n] The observed gas-phase value is from ref 25.

here. Nevertheless, the agreement with experiment appears to be fairly good except for ν(CH) which shows a difference of 92 cm^{-1} between the observed (liquid) and calculated (vapor) values. This cannot be ascribed to Fermi resonance since the $\delta(C-H)$ overtone is well separated from the $\nu(C-H)$ fundamental. As a check, a B3LYP/6-31G* calculation was done for free 2-propanol, and $\nu(C-H)$ = 2944 cm^{-1} was found after the scaling described above. The agreement with experiment (gas-phase $\nu(C-H)$ = 2875 cm^{-1}, ref 30) is again significantly worse than for other modes. Since the discrepancy in $\nu(C-H)$ is not unique to Sarin and is not reflected in other normal modes, it will be neglected in subsequent discussions.

The gas-phase value of $\nu(P{=}O)$ is of special interest since it is the mode most affected by adsorption (see below). For the Sarin analog (iPrO)(iPr)P(=O)(F), where iPr ≡ isopropyl, the gas-phase $\nu(P{=}O)$ is found[31] at about 1308 cm^{-1} vs 1277 cm^{-1} for liquid Sarin. Similarly, if the shift of 34 cm^{-1} in $\nu(P{=}O)$ between liquid and gas-phase DMMP is applied to liquid Sarin, an estimate of $\nu(P{=}O)$ = 1311 cm^{-1} is obtained for gas-phase Sarin. Hence $\nu(P{=}O)$ for gas-phase Sarin is estimated to fall in the range of 1308−1311 cm^{-1}.

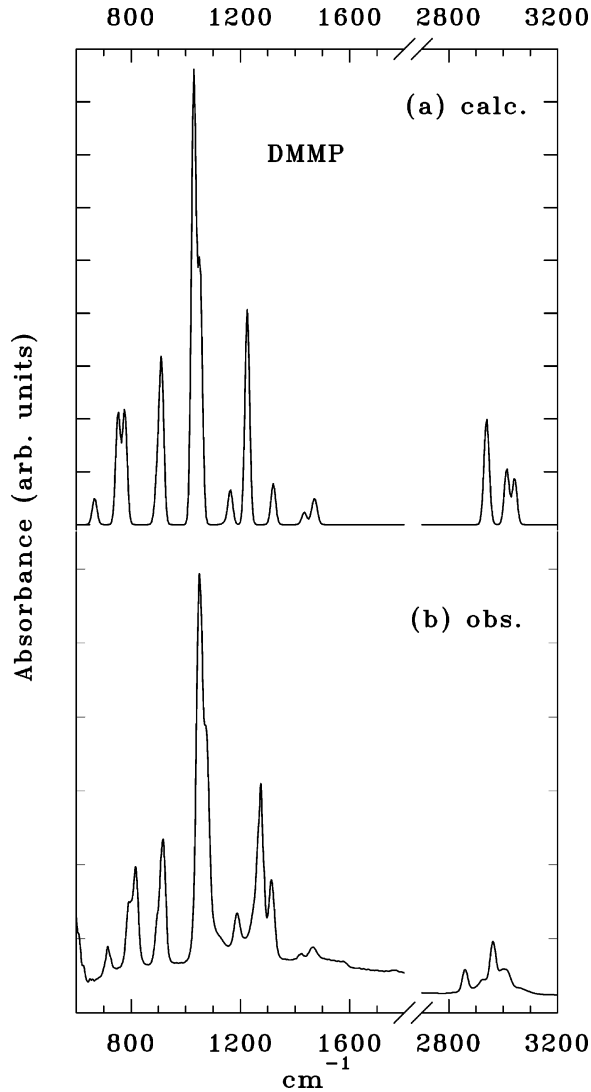

Figure 2. Calculated (a) and observed (b) gas-phase IR absorbance data for DMMP. The calculation is at the B3LYP/6-31G* level, and the normal-mode frequencies have been scaled as described in the text. The experimental spectrum was obtained at 8 cm^{-1} resolution at a DMMP pressure of 0.58 Torr in a 30-cm gas cell with KBr windows (ref 28).

2.2. The γ-Al_2O_3 Model. Since the construction of the surface model is an important issue, it will be examined in some detail. The bulk and surface structures of γ-Al_2O_3 have been analyzed in detail in the theoretical work of Pinto et al.[32,33] The bulk lattice model proposed in this work is a so-called "defective spinel" structure formed by first combining three primitive unit cells of the cubic spinel ($MgAl_2O_4$) lattice to give a stoichiometry of $Mg_6Al_{12}O_{24}$ in which Mg occupies tetrahedral (T_d) sites and Al fills octahedral (O_h) sites. All Mg is then replaced with Al, and two Al's are removed to give 8(Al_2O_3). There are 17 possible inequivalent pairs of T_d and/or O_h sites that can be emptied to form the two vacancies, each corresponding to a different lattice structure. Total-energy calculations[32] have identified the lowest-energy structure,[34] shown in Figure 3, which is one of those involving two O_h vacancies. The vacancy positions are important in determining the energies of the different surface planes since the lowest-energy surfaces are usually those that cut through a high number of vacancies. The structure is monoclinic (space group C2/m), and the primitive

TABLE 4: Observed and Calculated Mid-IR-Active Fundamental Frequencies (cm^{-1}) for Sarin

mode[a]	obs. (liq.)	calc. (gas)[b]
$\nu_a(CH_3)$[c]	2985	3016 (iPr)
$\nu_s(CH_3)$[c]	2932	2940 (iPr)
ν(CH)	2878	2970
$\delta_a(CH_3$, iPr)	1468	1479
$\delta_a(CH_3$, iPr)	1461	1466
$\delta_a(PCH_3)$	1419	1434
$\delta_s(CH_3$, iPr)	1390	1393
$\delta_s(CH_3$, iPr)	1380	1381
δ(CH)	1351	1342
$\delta_s(PCH_3)$	1320	1329
ν(P═O)[d]	1277	1255
$\rho(CH_3$, iPr)[e]	1180	1168
$\rho(CH_3$, iPr)[e]	1145	1126
$\rho(CH_3$, iPr)[e]	1106	1101
ν(C−O)[f]	1014	971
$\rho(PCH_3)$	921	925
$\rho(PCH_3)$	905	904
ν_s(C−C−C)	884	861
ν(P−F)	835	815
ν(P−C)	778	740
ν(P−O)[g]	721	695

[a] Mode assignments and experimental frequencies are from ref 29 for *liquid* Sarin. See Table 3, note (a), for definitions of notations. "iPr" refers to isopropyl. [b] B3LYP/6-31G*, calculated *gas-phase* frequencies scaled by a factor of 0.9613. [c] The ν_a and ν_s modes are those of the isopropyl group. The intensities of the corresponding P−CH_3 modes are calculated to be much weaker. The calculated in-plane and out-of-plane $\nu_a(CH_3)$ modes are nearly degenerate, and small splittings (a few wavenumbers) between in-phase and out-of-phase linear combinations are ignored. [d] In gas-phase (iPrO)(iPr)P(═O)(F) this mode occurs at ~1308 cm^{-1} (ref 31). [e] The multiple values given are for various in-phase and out-of-phase linear combinations of $\rho_{||}$ and $\rho_{\perp}$ modes. [f] Based on the calculated atomic displacements, this mode is better described as an "out-of-phase P−O−C stretch". [g] Based on the calculated atomic displacements, this mode is better described as an "in-phase P−O−C stretch".

unit cell constants are[32] $a = b = 5.663$ Å, $c = 13.712$ Å, $\alpha = \beta = 90.6°$, $\gamma = 60.401°$. The corresponding conventional unit cell parameters are $a = 9.789$ Å, $b = 13.712$ Å, $c = 5.697$ Å, $\alpha = \beta = 90°$, $\gamma = 90.69°$.

Other theoretical investigations[35−42] of γ-Al_2O_3 have been reported which differ in the description of the bulk lattice. A particular point of disagreement, discussed at length in recent publications, concerns whether γ-Al_2O_3 is better described by a spinel model,[42] as noted above, or by a nonspinel structure[40] (see also ref 43). We have used the results of Pinto et al.[32,33] since, other than the work of Digne et al.,[38] this is the only ab initio study of which we are aware that deals specifically with the structures of different surfaces. The bulk model[37] from which the surface models of Digne et al.[38] are derived has recently been questioned,[42] although it is not possible at present to obtain a clear resolution of the controversy regarding the bulk structure.[43]

Calculations[32] of the surface energy for different surface planes[44] after relaxation (σ_R) have found the lowest in energy to be the (111)*a* ($\sigma_R = 0.95$ J m^{-2}), shown in Figure 4, which is terminated in T_d cation sites. This surface is formed by "cleaving" on the layer of vacancies shown at the middle of the unit cell in Figure 3, and relaxation involves relatively small displacements confined mainly to the outermost Al and O planes and mainly in the surface-normal direction. The relaxed (001) plane is a close second in stability, with $\sigma_R = 1.05$ J m^{-2}, and is terminated in O_h and T_d sites in a 3:1 concentration ratio. The ideally terminated (001) surface is unstable and undergoes large and complex atomic displacements in the course of relaxation. The (110) surface, which is usually considered[45] to be the chemically active surface in γ-Al_2O_3 powders, has a relatively high surface energy ($\sigma_R = 1.53$ J m^{-2}) and also exhibits large and complex displacements during relaxation.

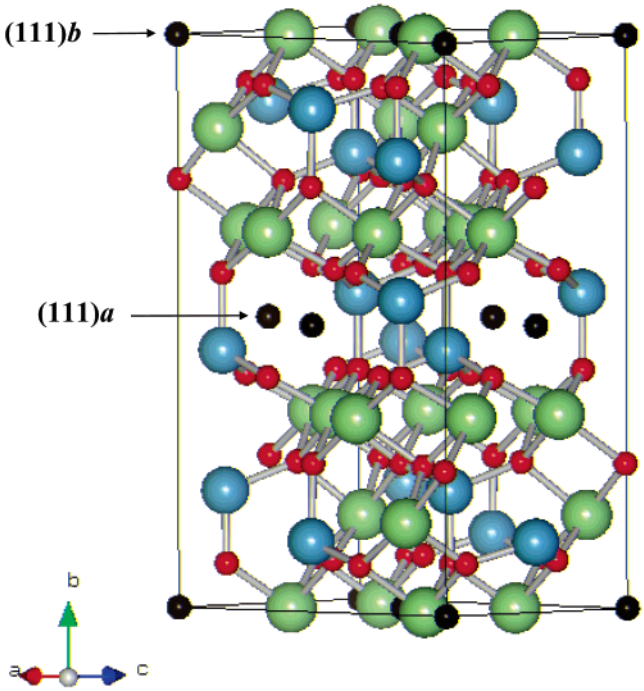

Figure 3. Calculated (ref 32) lowest-energy form of the bulk γ-Al_2O_3 conventional unit cell. Al(T_d), Al(O_h), and O atoms are shown in blue, green, and red, respectively. The small black spheres not bonded to anything indicate the vacancies used to form the defective spinel structure (see text). The arrows indicate where "cleaving" occurs to form the (111)*a* and (111)*b* planes as discussed in ref 32.

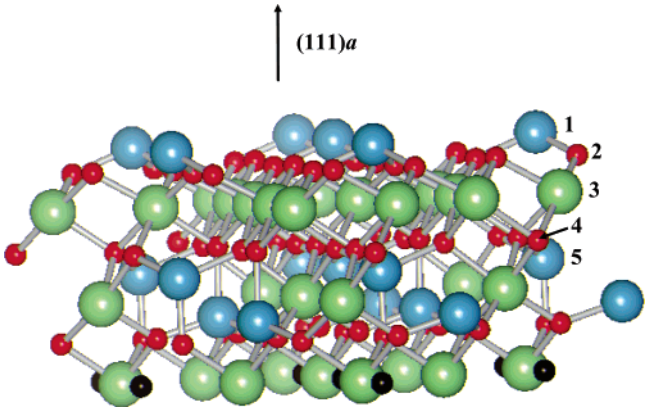

Figure 4. Schematic diagram of the unrelaxed (ideally terminated) (111)*a* surface described in ref 32. The surface normal lies in the plane of the page. As noted in the text, the (111) label applies to the cubic spinel lattice. In terms of the conventional unit cell of γ-Al_2O_3 (Figure 3), the surface plane is the (010). The small black spheres in the lower-most Al(O_h) layer represent vacancies. For clarity, only half of one unit cell in the (111) direction is shown. The numbers to the right label the crystal planes, with 1 being the surface. For clarity, small inequivalences among atoms in some planes, as to the exact position along the surface normal, are neglected in numbering the planes.

The discussion thus far has concerned only the fully dehydroxylated surface. However, −OH groups can be important in the surface chemistry of oxides, and the question arises of how to model the hydroxylated γ-Al_2O_3 surface.[46] For the (111)-*a* this has been addressed[33] by examining the dissociative adsorption of H_2O which yields surface Al-OH and −OH

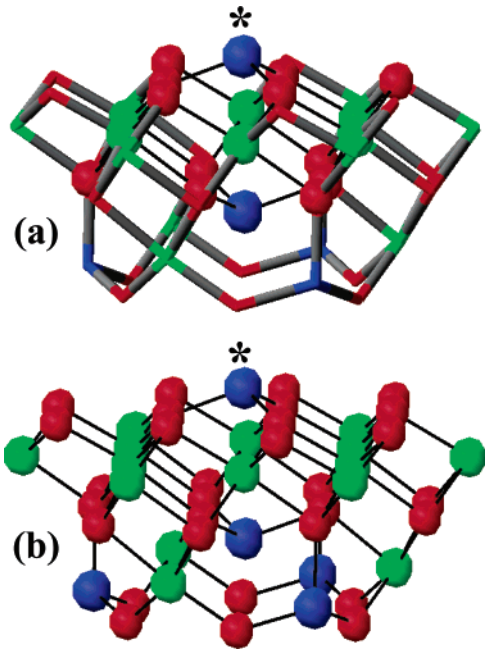

Figure 5. (a) Small Al_8O_{12} and (a) large $Al_{20}O_{30}$ cluster models. The coloring of Al(T_d), Al(O_h), and O atoms is the same as in Figures 3 and 4. In (a), the positions of the additional atoms used to form the large system are shown by the tube intersections. In either case the asterisk marks the Al(T_d) surface site at which adsorption occurs.

groups. Although adsorption on the hydroxylated surface will not be considered in the present study, the model can readily be expanded to include such effects.

In the following investigation, the (111)*a* surface (Figure 4) will be used to model adsorption on γ-Al_2O_3. The (111)*a* is the simplest and most stable of the γ-Al_2O_3 surfaces (in the model of Pinto et al.[32,33]), and the terminating, singly unsaturated Al(T_d) sites are strong Lewis acids. Such Lewis acid sites are an essential feature in the chemisorption processes to be studied here. The model cluster was formed by first "cleaving" to expose the (111)*a* surface (Figure 3). Atomic displacements from the bulk positions during relaxation are known[32] to be small in all directions beyond the second Al plane (layer number 3 in Figure 4). Two different model clusters, Al_8O_{12} and $Al_{20}O_{30}$ (Figure 5), were cut from the slab and used to represent the chemically active region. Both are stoichiometric and charge-neutral.[47,48] The Al_8O_{12} cluster is essentially the same as that used previously[49] to study adsorption of H_2O on the α-Al_2O_3 (0001) surface and is only somewhat larger than the minimum (Al_4O_6) needed to model a chemically active surface Al(T_d) site. The larger model, on the other hand, was designed so that none of the O ions adjacent to the central Al(T_d) surface site are themselves at the edge of the cluster. Thus, the $Al_{20}O_{30}$ cluster may be viewed as an Al_8O_{12} cluster "embedded" in a very small host lattice having the γ-Al_2O_3 structure.

The dimensions of the surface plane of the larger cluster are more nearly comparable to those of the adsorbate species of interest, whereas such molecules extend beyond the edges of the Al_8O_{12} cluster. The importance of edge effects in small-cluster models has been noted previously[50] in connection with the adsorption of H_2O on α-Al_2O_3 (0001). The Al_8O_{12} cluster, either alone or when incorporated into the $Al_{20}O_{30}$ cluster, is treated using 6-31G* or larger basis sets (see below). The additional atoms making up the $Al_{20}O_{30}$ cluster are treated using 3-21G basis sets. This mixed-basis-set approach has been used

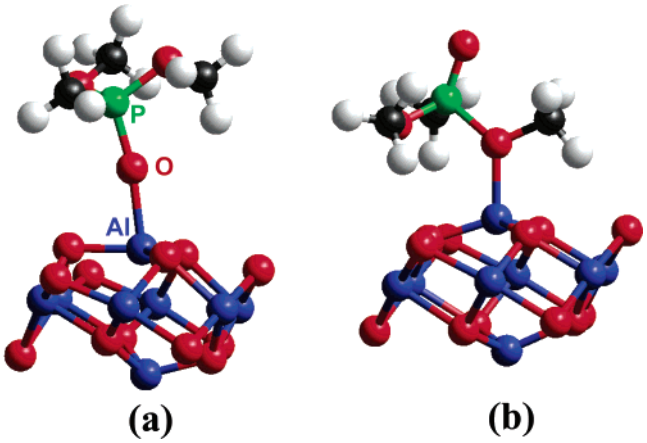

Figure 6. Schematic diagrams showing the structures (not optimized) for DMMP adsorbed via (a) the P═O group and (b) the CH_3−O−P group. For simplicity, only the Al_8O_{12} cluster is shown. In this case, both Al(T_d) and Al(O_h) sites (cf. Figure 5a) are shown in blue.

successfully in other surface calculations involving oxide clusters, e.g., for α-Al_2O_3 (0001) (ref 49) and CeO_2 (110) (ref 51).

Geometry optimization was confined to the adsorbate, the active Al site (marked by the asterisk in Figure 5) and the three O nearest-neighbors of this site. The rest of the cluster remained fixed in positions corresponding to the ideally terminated bulk lattice. This is a widely used approach to geometry optimization in clusters since relaxation of larger segments often results either in failure to converge or in structures that are severely distorted relative to periodic-slab surface models. In spite of the approximate nature of this treatment, the results for the bare (i.e., adsorbate-free) surface agree fairly well with those of periodic slab calculations.[32] The surface Al(T_d) atom undergoes an inward displacement of 0.22 Å along the surface normal and a slight displacement (~0.02 Å) in the surface plane. The corresponding periodic-slab results are about 0.33 Å inward and 0.028 Å laterally. For the nearest-neighbor O atoms the present result is an outward displacement of 0.02 Å and a lateral motion of about 0.02 Å. The corresponding periodic-slab results are 0.08 Å outward and 0.01 Å laterally.

The electrostatic potential (EP) in the vicinity of the adsorption site, due to ions in the semi-infinite crystal lattice (i.e., the Madelung potential), is a subject of concern in cluster treatments of ionic materials, particularly for small clusters or in the adsorption of polar molecules.[52] Various methods for dealing with the EP range from complete neglect (i.e., a free-standing cluster) to sophisticated approaches[53−57] in which the model cluster is embedded in an array of point charges carefully designed to produce the correct EP near the adsorption site (termed "charge embedding"). In most cases, the cluster is surrounded by an intermediate region described in terms of a shell model,[53] bare pseudopotentials, or model ion potentials[58] rather than point charges. The EP is neglected in the present work; however, tests will be performed which suggest that the free-standing $Al_{20}O_{30}$ cluster gives reliable results in the present application.

2.3. DMMP Adsorbed on γ-Al_2O_3. The chemical interaction of DMMP with γ-Al_2O_3 powder has been studied by Mitchell et al.[59] Studies have also been reported for adsorption on an unspecified form of Al_2O_3 powder,[60] on oxide layers on polycrystalline Al films,[61] and on an oxide layer on an Al(111) surface.[62] At room temperature, a nondissociative, dative-bonding interaction occurs between the Al Lewis acid site and the O atom of the molecular P═O group (Figure 6a). Surface

TABLE 5: Basis-Set and Cluster Size Dependence of Results for Adsorption of DMMP on γ-Al_2O_3

cluster/ basis set	ΔE_{ads}[a]	r(Al−OP)	r(AlO═P)	∠(Al−O−P)
Al8O12/ 6-31G*[b]	−56.1 (−47.1)	1.827	1.523	147.4
Al20O30/ 6-31G*[c]	−66.5 (−51.1)	1.802[d]	1.529[e]	150.1
Al20O30/ 6-31+G*[c]	−70.8[e] (−53.5)	1.795	1.527	151.6
Al20O30/ 6-311G(df)[f]	−74.2 (−57.5)	1.788	1.519	151.1

[a] ΔE_{ads} is in kcal/mol, bond lengths are in Ångstroms and the bond angle is in degrees. Values in parentheses are BSSE-corrected (ΔE^{C}_{ads}) results. ΔE_{ads} has not been corrected for ZPE. [b] 6-31G* basis sets were used for DMMP and for the entire Al_8O_{12} cluster. [c] The basis set indicated was used for the Al_8O_{12} sub-cluster and for the DMMP. The additional atoms forming the $Al_{20}O_{30}$ cluster were treated with 3-21G basis sets. [d] The calculated (6-31G*) Al−O distance from the adsorption site to the nearest-neighbor lattice O atoms is 1.770 Å. [e] The calculated (6-31G*) P−OCH_3 and P═O distances in free DMMP are 1.622 and 1.486 Å, respectively. [f] The molecule and the central Al(−O−)$_3$ surface site, at which adsorption occurs, are treated using 6-311G(df) basis sets. The remainder of the Al_8O_{12} cluster is treated with 6-31G* basis sets, and additional atoms of the $Al_{20}O_{30}$ cluster are treated with 3-21G basis sets.

−OH groups, if present, may also be involved through hydrogen-bonding to the molecular −OCH_3 group(s). Raising the temperature leads to a nucleophilic attack by the O atom of the −OH site on the P atom, causing the release of CH_3OH and the formation of a bidentate structure with an Al−O−P bond in addition to the Al−O═P dative bond. In room-temperature IR data, only the ν(P═O) mode, at 1216 cm^{-1}, exhibits a substantial shift from the gas-phase DMMP value (1276 cm^{-1}). Other modes appear at energies close to those found in gas-phase DMMP.

The γ-Al_2O_3 model described above was tested using the adsorption energy (ΔE_{ads}) of DMMP in the Al−O═P dative-bond configuration as a point of reference. Here

$$\Delta E_{ads} = E(\mathrm{DMMP} + Al_2O_3) - E(\mathrm{DMMP}) - E(Al_2O_3)$$

$$\Delta E^{C}_{ads} = \Delta E_{ads} + \Delta E_{BSSE}$$

where the first term in ΔE_{ads} is the energy of the adsorbate and the cluster and the next two terms are the energies of the bare cluster and the free DMMP molecule, respectively. All energies were obtained after geometry optimization under the conditions described above. In this and in the following section, ΔE_{ads} is not corrected for zero-point vibrational energy (ZPE); however, a counterpoise correction for basis set superposition error (ΔE_{BSSE}) is applied. A negative ΔE^{C}_{ads} corresponds to an exothermic process.

First, ΔE^{C}_{ads} was obtained for the Al_8O_{12} and $Al_{20}O_{30}$ clusters to check the effect of the size of the model. The results (for 6-31G* basis sets) shown in Table 5 indicate a somewhat weaker interaction for the smaller cluster which is reflected in both the smaller ΔE_{ads} and the longer r(Al−OP). Hence, subsequent work will make use of the larger cluster. Next, the basis-set dependence of ΔE_{ads} was tested for the $Al_{20}O_{30}$ cluster by comparing results obtained with 6-31G* vs 6-31$^+$G* for DMMP and for the Al_8O_{12} sub-cluster. In both cases, as noted above, 3-21G basis sets were used for the atoms added to Al_8O_{12} to make the $Al_{20}O_{30}$ cluster. The results (Table 5) show a small increase in the adsorption energy and a slightly shorter r(Al−OP) for 6-31$^+$G*, indicating a stronger interaction. The basis-set quality was further increased using 6-311G(df) for DMMP and for the Al(−O−)$_3$ center where adsorption occurs (cf. Figure 5). As before, the rest of the Al_8O_{12} cluster was treated with 6-31G* basis sets, and the additional atoms making up the $Al_{20}O_{30}$ cluster were treated with 3-21G basis sets. The results show a further small increase in ΔE_{ads} and shortening of r(Al−OP).

All models and basis sets in Table 5 show a substantial BSSE. This is especially true for the $Al_{20}O_{30}$ cluster, where ΔE_{BSSE} is in the range of 15.4−17.3 kcal/mol and does not decrease when larger basis sets are used for DMMP and for the reactive region. Part of this effect is associated with the use of 3-21G basis sets for the peripheral atoms, as described above. A calculation with 6-31G* basis sets for DMMP and for the entire $Al_{20}O_{30}$ cluster gave ΔE_{BSSE} = 10.6 kcal/mol, close to the value of 9.0 kcal/mol found for the Al_8O_{12} cluster (Table 5). This large value of ΔE_{BSSE}, in proportion to ΔE_{ads}, could cast doubt on the geometry optimization,[63] which does not include BSSE in evaluating the total energy. However, Table 5 shows that there is little difference between the Al_8O_{12} and $Al_{20}O_{30}$ clusters, regarding the geometry of the chemisorption bond, when both are treated at the 6-31G* level even though ΔE_{BSSE} = 9.0 kcal/mol for the former and 15.4 kcal/mol for the latter. In this comparison, the Al_8O_{12} sub-cluster of the $Al_{20}O_{30}$ is treated with 6-31G* basis sets and the rest with 3-21G.

The third test examined an alternative adsorption geometry. The calculations thus far all began with the DMMP positioned directly above the central Al site with the P═O bond orientation and Al−O═P distance approximately correct for dative bond formation (Figure 6a). Another a priori reasonable geometry places the O atom of one of the P−O−CH_3 groups directly above the Al site (Figure 6b). Adsorption via Al−O dative bond formation to a CH_3O− group is inconsistent with the IR data cited above, but it is nevertheless necessary to test the predicted ΔE_{ads} for this structure. This was done using the smaller (Al_8O_{12}) cluster with 6-31G* basis sets, and ΔE_{ads} = −39.6 kcal/mol was obtained, with r(Al−O) = 1.91 Å, vs −56.1 kcal/mol for Al−O═P using the same model (cf. Table 5). Thus, the calculations agree with experiment that Al−O═P is the energetically favored adsorption geometry. A bidentate structure, with one Al forming an Al−O═P bond and another forming an Al−O bond to a methoxy group, was not included in the present model, which involves only one Al surface site. Given the Al−Al nearest-neighbor distance on the model surface (5.663 Å, Figure 4) and the various bond lengths shown in Table 5, such a structure would not be possible without a severe bond-angle distortion of the approximately tetrahedral P bonding.

Another test consisted of computing the molecular (i.e., nondissociative) adsorption of H_2O on the model cluster for comparison with the periodic-slab result[33] of ΔE_{ads} = −1.22 eV (−28.1 kcal/mol) for the (111)*a* surface of γ-Al_2O_3. This tests the quality of the free-standing cluster result for the difficult case of a relatively weak interaction with a polar molecule. The structure was optimized, as described above, at the B3LYP level with 6-31$^+$G* basis sets for H_2O and for the Al_8O_{12} sub-cluster and 3-21G basis sets for the rest of the $Al_{20}O_{30}$ cluster. The resulting Al−OH_2 distance was 1.928 Å. A single-point calculation was then done with 6-31$^+$G* basis sets for all atoms, and ΔE_{ads} = −35.1 kcal/mol was obtained after applying the BSSE correction of +6.0 kcal/mol. The difference of 7.0 kcal/mol from the periodic-slab result, while not trivial, is comparable to the scatter among various embedded-cluster and periodic-slab results[64] for the molecular adsorption of H_2O on α-Al_2O_3

(0001), which has been the subject of several theoretical studies. Embedded-cluster (periodic-slab) results for this system fall in the range of −23.4 to −35.7 (−23.3 to −33.7) kcal/mol depending on method and basis sets and on the details of the model.

A final test concerns the possible role of "surface states" in the free-cluster results. Note the configuration of the first-underlayer Al atoms in Figures 5a,b, which correspond to "Layer #3" in Figure 4. In bulk γ-Al_2O_3 these are O_h sites. In the Al_8O_{12} cluster, these are missing two of the six O nearest-neighbors. In $Al_{20}O_{30}$ these same sites are now fully coordinated, but the additional first-underlayer Al atoms at the periphery are each missing three O nearest-neighbors. To determine whether this might affect the difference between the Al_8O_{12} and $Al_{20}O_{30}$ results in Table 5, a calculation was done in which one H atom was added to each of these six 3-fold-coordinated Al sites and allowed to relax during geometry optimization. The object was not to remove completely the "surface states" but to reduce the difference in this regard between the two clusters. For DMMP adsorption, $\Delta E_{ads} = -68.6$ kcal/mol was obtained, using 6-31G* basis sets, vs −66.5 kcal/mol (Table 5) without H. After BSSE correction, $\Delta E^{C}_{ads} = -53.9$ kcal/mol was obtained with H-termination vs −51.1 kcal/mol without. This difference of 5.5% is not considered to be significant in analyzing the adsorbate structure and is neglected. Casarin et al.[65] have discussed the use of "pseudo-H atoms", with fractional numbers of electrons, to saturate peripheral sites in α-Al_2O_3 model clusters, but this technique was not available in the present work.

Table 6 gives the computed vibrational modes of DMMP adsorbed on γ-Al_2O_3 together with the experimental results[59] at room temperature. Comparisons are made between the observed and calculated frequencies for adsorbed DMMP and between the shifts relative to the gas phase, i.e., [(obs. adsorbed) minus (obs. gas)] vs [(calc. adsorbed) minus (calc. gas)]. The computation used 6-31G* basis sets and the $Al_{20}O_{30}$ cluster in the manner described above. Obtaining normal-mode energies for larger basis sets was computationally intensive, and in any case, the free-molecule frequencies discussed above show very little change when the basis set is enlarged beyond 6-31G*. The atomic displacements associated with each adsorbate normal mode were examined and found to contain virtually no contribution from atoms in the $Al_{20}O_{30}$ cluster itself. Hence, the frequencies are considered reliable, within the basic limitations of the theory, even though only a partial geometry optimization of the cluster was performed (see above).

The average error of 2.1% in the calculated frequencies is essentially the same as that seen in Table 3 (1.9%) for free DMMP. The computed $\Delta\nu$(P═O), relative to the computed gas-phase frequency, is −84 cm^{-1} which is in reasonable agreement with the experimental value of −60 cm^{-1}. Also in agreement with experiment is the fact than none of the other modes show nearly as large a shift from the corresponding gas-phase value. The second-largest such affect appears in ν(C−O), where the calculation gives $\Delta\nu = -32$ (−27) cm^{-1} for the in-phase (out-of-phase) linear combination. The experimental work reports only one ν(C−O) for adsorbed DMMP, at 1058 cm^{-1}, but if that is ascribed to the in-phase mode (at 1075 cm^{-1} in the gas phase, Table 3) then the observed $\Delta\nu$(C−O) is −17 cm^{-1}. The only large discrepancy is in ν_a(P−CH_3), for which the observed and calculated shifts are in opposite directions. However, the agreement in the shift of the corresponding ν_s(P−CH_3) mode is essentially exact.

2.4. Sarin Adsorbed on γ-Al_2O_3. The adsorption of Sarin on γ-Al_2O_3 has been studied experimentally using IR spectroscopy,[29] and ^{31}P, ^{13}C, and ^{27}Al nuclear magnetic resonance data[66] have been reported for Sarin on Al_2O_3 nanoparticles. Initial adsorption occurs[29] via a strong Al−O═P interaction which, on an hydroxylated surface, is followed by H_2O elimination, transfer of F to an adjacent Al site, and formation of a bidentate phosphonyl structure. The kinetic aspects of the reaction of Sarin with γ-Al_2O_3 have also been studied.[67]

Three modes of adsorbate bonding have been considered in the present work; namely, Al−O═P, Al−F−P, and Al−O(iPr) where the last of these refers to bonding *via* the O of the isopropyl group. The results are shown in Table 7. As in the case of DMMP, and in agreement with experimental data[29] for Sarin, Al−O═P bond formation is energetically favored. The BSSE corrections for all three structures were obtained in order to verify that this conclusion remains unchanged. For the most stable structure, Al−O═P, Table 7 also gives results for the higher-quality 6-311G(df) basis sets which can be compared with those for DMMP in Table 5.

With 6-311G(df) basis sets, ΔE^{C}_{ads} for Sarin (−49.2 kcal/mol) is smaller than that of DMMP (−57.5 kcal/mol), a difference of 8.3 kcal/mol. It is noteworthy that virtually the same difference in ΔE^{C}_{ads}, 8.8 kcal/mol, is seen for 6-31G* basis sets, again using the $Al_{20}O_{30}$ cluster (cf. Tables 5 and 7). Before BSSE correction, the difference in ΔE_{ads} between DMMP

TABLE 6: Observed and Calculated Mid-IR-Active Fundamental Frequencies (cm^{-1}) for DMMP Adsorbed on γ-Al_2O_3

mode[a]	observed[a]	calculated[b]	|error|[c]
ν_a(P−CH_3)	2996 (−18)	3053 (+11)	0.0190
ν_a(O−CH_3)[d]	2956 (−6)	3085 (i.p.)	
ν_s(P−CH_3)	2929 (+8)	2966 (+8)	0.0126
ν_s(O−CH_3)	2853 (−6)	2989	
δ_a(O−CH_3)[e]	1465 (−6)	1470 (0)	0.0034
δ_s(O−CH_3)	1450	1440	0.0069
δ_a(P−CH_3)[f]	1423 (0)	1428	0.0035
δ_s(P−CH_3)	1314 (−1)	1331 (+11)	0.0129
ν(P═O)	1216 (−60)	1141 (−84)	0.0617
ρ(O−CH_3)[g]	1190 (+2)	1163 (0)	0.0227
ν(O−C)[h]	1058 (−17)	1021 (−32)	0.0350
ρ(P−CH_3)[i]	904 (+15)	934 (+23)	0.0332

[a] Mode assignments and observed frequencies (recorded at 30 °C) are from ref 59. See Table 3, footnote a, for definitions of notations. Shifts relative to the observed gas-phase values (cf. Table 3) are given in parentheses. [b] This work, using the $Al_{20}O_{30}$ cluster with 6-31G* basis sets for DMMP and for the Al_8O_{12} sub-cluster and 3-21G basis sets for the rest of the cluster. The frequencies have been scaled by a factor of 0.9613 (ref 19). Shifts relative to the calculated gas-phase values (cf. Table 3) are given in parentheses. Shifts for ν(O−CH_3) are not given because Fermi resonance with the δ(O−CH_3) is not included in the calculation (see text). [c] Errors in the absolute frequencies are defined as |calc.- obs.|/obs. The average error for the ten modes considered is 0.021 (i.e., 2.1%) in magnitude. [d] The in-plane (i.p.) mode is calculated to be more intense than the out-of-plane (o.p.) mode. Hence, the observed mode is assigned to the i.p. Small splittings (a few wavenumbers) between in-phase and out-of-phase linear combinations of ν(O−CH_3) and other modes are ignored. [e] The calculated value is an average of closely spaced (over a range of 13 cm^{-1}) in-phase and out-of-phase linear combinations of i.p. and o.p. modes. [f] Reference 59 assigns this mode to δ_a(P−CH_3) which is believed to be correct. See Table 3, footnote i. [g] Only one ρ(O−CH_3) is reported in the experimental data. The calculated value given is for the $\rho_{||}$ mode. The calculated energy of the $\rho_{\perp}$ mode is 1128 cm^{-1}. See Table 3, footnote k. [h] Only one ν(C−O) mode is reported in the experimental data. The calculated value given is for the in-phase linear combination. The calculated energy of the out-of-phase combination is 1003 cm^{-1}. [i] Only one ρ(CH_3) is reported in the experimental data. The calculated value given is for the $\rho_{||}$ mode. The calculated energy of the $\rho_{\perp}$ mode is 922 cm^{-1}. See Table 3, footnote m.

TABLE 7: Results for the Adsorption of Sarin on γ-Al_2O_3[a]

structure	ΔE_{ads}	ads. bond[b]	ads. angle[c]	r(P−F)	r(P═O)	r(P−O)
free sarin[d]				1.600	1.478	1.604
Al−O═P[d]	−56.6 (−42.3)	1.822	141.3	1.573	1.517	1.557
Al−F−P[d]	−36.1 (−25.1)	1.839	135.0	1.801	1.472	1.568
Al−O(iPr)[d]	−41.1 (−24.5)	1.912	124.7	1.581	1.477	1.707
Al−O═P[e]	−65.1 (−49.2)	1.805	149.0	1.563	1.503	1.545

[a] All results are computed using the B3LYP functional and the $Al_{20}O_{30}$ cluster. Bond lengths are in Ångstroms, and bond angles are in degrees. ΔE_{ads} is in kcal/mol. [b] This is the Al−X distance (X═O or F). [c] This is the Al−X−P bond angle (X═O or F). [d] 6-31G* basis sets were used for Sarin and for the Al_8O_{12} sub-cluster. Additional atoms forming the $Al_{20}O_{30}$ cluster were treated with 3-21G basis sets. The ΔE^C_{ads} values are given in parentheses. No ZPE corrections have been applied. [e] The basis sets used were 6-311G(df) for Sarin and for the Al(−O−)$_3$ adsorption site, 6-31G* for the rest of the Al_8O_{12} cluster and 3-21G for the additional atoms forming the $Al_{20}O_{30}$ cluster.

TABLE 8: APT Atomic Charges in Free DMMP and Sarin[a]

molecule	P*═O	P═O*	RO*[b]	P−F*
DMMP	+2.17	−0.87	−1.03	
Sarin	+2.19	−0.84	−1.12	−0.68

[a] All values are obtained at the B3LYP/6-311G(df) level. The asterisk marks the atom being described. [b] R≡CH_3 for DMMP and $(CH_3)_2CH$ for Sarin.

and Sarin is 9.9 (9.1) kcal/mol for the smaller (larger) basis sets. The similarity of these results indicates that the comparison between DMMP and Sarin is essentially unaffected by systematic errors, if any, in the model and by the large BSSE corrections.

The reason for the smaller ΔE_{ads} for Sarin is not readily apparent. Table 8 summarizes the atomic charges computed for free DMMP and Sarin at the B3LYP/6-311G(df) level using the atomic polar tensor (APT) method.[68] A smaller charge on the O atom of the P═O group, due to the electronegative F atom, could explain the smaller ΔE_{ads} for Sarin, but Table 8 shows little difference from DMMP in this regard. The steric effect of the isopropyl group in Sarin is not believed to be a factor since the optimized structure (not shown) places this group well away from the surface. Also, adsorbed Sarin remained in the low-energy conformation shown in Figure 1b without being forced into another, less stable configuration[17,18] (which would have made ΔE_{ads} less negative).

Table 9 gives the computed vibrational frequencies for Sarin adsorbed in the Al−O═P configuration. As in the case of DMMP, the normal-mode calculation was performed for adsorption on the $Al_{20}O_{30}$ cluster using 6-31G* basis sets for Sarin and for the Al_8O_{12} sub-cluster. The agreement between observed and calculated frequencies is surprisingly good. The average error of 1.2% is less than the error of 2.1% (Table 6) for adsorbed DMMP. As in the case of DMMP the largest error (about 6%) is in ν(P═O). For Sarin, the comparison between observed and calculated adsorption-induced mode shifts is hampered by the lack of gas-phase data. The estimate (see above) of 1311 cm^{-1} for the gas-phase ν(P═O) frequency yields $\Delta\nu$(P═O) = −66 cm^{-1}. This is to be compared with the calculated shift (calc. adsorbed minus calc. gas) of −86 cm^{-1}.

The calculated adsorption-induced shifts for other modes are much less than $\Delta\nu$(P═O), in general agreement with the Sarin data. Comparing the calculated values in Tables 4 and 9, one finds that such shifts are typically <15 cm^{-1} in magnitude. One exception is the ν(C−O) mode, for which the calculated shift (adsorbed minus gas) is +36 cm^{-1}, whereas the observed shift (adsorbed minus liquid) is only +6 cm^{-1}. However, the observed

TABLE 9: Observed and Calculated Mid-IR-Active Fundamental Frequencies (cm^{-1}) for Sarin Adsorbed on γ-Al_2O_3

mode[a]	observed[a]	calculated[b]	|error|[c]
$\nu_a(CH_3)$[d]	2980	3015 (iPr, o.p.)	0.0117
$\nu_s(CH_3)$	2930	2941 (iPr)	0.0038
ν(CH)[e]	2870	3068	
$\delta_a(CH_3$, iPr)	1465	1471	0.0041
$\delta_a(CH_3$, iPr)	1455	1463	0.0055
$\delta_a(PCH_3)$	1415	1428	0.0092
$\delta_s(CH_3$, iPr)	1380	1386	0.0043
$\delta_s(CH_3$, iPr)		1379	
δ(CH)	1350	1349	0.0007
$\delta_s(PCH_3)$[f]	1320	1335	0.0114
$\delta_s(PCH_3)$[f]	1315		
ν(P═O)[g]	1245	1169	0.0610
$\rho(CH_3$, iPr)	1170	1176	0.0051
$\rho(CH_3$, iPr)	1135	1139	0.0035
$\rho(CH_3$, iPr)	1110	1089	0.0189
ν(C−O)	1020	1007	0.0127

[a] Mode assignments and observed frequencies are from ref 29. "iPr" refers to isopropyl. See Table 3, note (a), for definitions of notations. [b] This work, using the $Al_{20}O_{30}$ cluster with 6-31G* basis sets for Sarin and for the Al_8O_{12} sub-cluster and 3-21G basis sets for the rest of the cluster. The "raw" frequencies have been scaled by a factor of 0.9613 (ref 19). [c] Errors are defined as in Table 6, footnote c. The average error is 0.012 (1.2%). [d] The isopropyl $\nu_a(CH_3)$ in-plane (i.p.) modes, calculated to occur at 3035 cm^{-1}, are computed to be weak relative to the out-of-plane (o.p.) modes. Hence the observed feature is assigned as o.p. Small splittings (a few wavenumbers) between the calculated in-phase and out-of-phase linear combinations of the $\nu(CH_3)$ modes are ignored. For the P−CH_3 group, ν_a (3042 cm^{-1}) and ν_s (2964 cm^{-1}) are computed to be much weaker than for the isopropyl group and are not assigned to any observed feature. [e] See text for a discussion of ν(CH). [f] Peaks observed at 1320 and at 1315 cm^{-1} were both assigned to $\delta_s(PCH_3)$; however, only one such mode is found among the calculated normal modes. [g] For an estimated gas-phase frequency of ∼1311 cm^{-1} (see text), an experimental $\Delta\nu$(P═O) = −66 cm^{-1} is obtained for the adsorbed molecule. The corresponding calculated value (i.e., calc. adsorbed minus calc. gas-phase) is −86 cm^{-1}.

and calculated ν(C−O) values for adsorbed Sarin in Table 9 show fairly good agreement (a 13 cm^{-1} difference), whereas the observed (liquid) and calculated (vapor) values for free Sarin in Table 4 do not (a 43 cm^{-1} difference). This leads one to suspect that ν(C−O) in the vapor may be significantly lower than in the liquid. A much larger discrepancy occurs for ν(C−H) where the observed and calculated values for adsorbed Sarin (Table 9) differ by 198 cm^{-1}. The comments made above regarding ν(C−H) in free Sarin also apply here.

3. Summary

Ab initio quantum-chemical calculations have been performed to study the interaction of DMMP and Sarin with γ-Al_2O_3. Emphasis has been placed on a detailed comparison between calculated and observed (mainly IR spectroscopic) results for the adsorbed species. The results are as follows.

(1) Free-standing Al_8O_{12} and $Al_{20}O_{30}$ clusters give reasonable descriptions of the adsorbate structure and properties. In both cases, Al−O═P dative-bond formation is the energetically favorable adsorption geometry, and the IR spectra are in general agreement with experiment. Equally important is the fact that competing geometries, which are contra-indicated by experiment, are found to be energetically unfavorable.

(2) The results are not strongly dependent on the quality of the basis sets. For DMMP adsorption on the $Al_{20}O_{30}$ cluster, ΔE^C_{ads} at the B3LYP/6-31G* level is about 12% smaller than at the B3LYP/6-311G(df) level. The length and angle of the chemisorption bond show little variation between the two

extremes. Likewise, the dependence on cluster size is not strong. With 6-31G* basis sets, ΔE^{C}_{ads} for DMMP adsorption is about 8% smaller for the Al_8O_{12} than for the $Al_{20}O_{30}$ cluster.

(3) "Side-by-side" comparison of the ab initio results for DMMP and Sarin indicates that DMMP is a reasonably good simulant. In either case, the energetically favorable geometry for adsorption on γ-Al_2O_3 is the same. The adsorption energies are comparable ($\Delta E^{C}_{ads} = -57.5$ kcal/mol for DMMP and -49.2 kcal/mol for Sarin, both for $Al_{20}O_{30}$ at the B3LYP/6-311G(df) level). However, for reasons which are unclear at present, ΔE^{C}_{ads} is about 8.3 kcal/mol greater for DMMP than for Sarin.

(4) The calculated normal-mode frequencies for DMMP and Sarin, both free and adsorbed on γ-Al_2O_3, have been used to verify the reported mode assignments[23,24,29,59] for the mid-IR spectra of these systems. Since the calculation provides a physical picture of the atomic displacements in each mode, the interpretations are unambiguous in most cases.

Acknowledgment. We are indebted to H. P. Pinto for help in setting up the structural model for γ-Al_2O_3 and to B. I. Dunlap and A. Michalkova for helpful discussions. This work was supported by the Defense Threat Reduction Agency and by a grant of computer time from the DOD High-Performance Computing Modernization Program at the ASC-MSRC, Wright-Patterson AFB.

References and Notes

(1) Wang, J.; Gu, J.; Leszczynski, J. *J. Phys. Chem. B* **2006**, *110*, 7567.
(2) Šečutė, J.; Menke, J. L.; Emnett, R. J.; Patterson, E. V.; Cramer, C. J. *J. Org. Chem.* **2005**, *70*, 8649.
(3) Michalkova, A.; Ilchenko, M.; Gorb, L.; Leszczynski, J. *J. Phys. Chem. B* **2004**, *108*, 5294.
(4) Michalkova, A.; Gorb. L.; Ilchenko, M.; Zhikol, O. A.; Shishkin, O. V.; Leszczynski, J. *J. Phys. Chem. B* **2004**, *108*, 1918.
(5) Hurley, M. M.; Wright, J. B.; Lushington, G. H.; White, W. E. *Theor. Chem. Acc.* **2003**, *109*, 160.
(6) Zheng, F.; Zhan, C. G.; Ornstein, R. L. *J. Chem. Soc. Perkin Trans. 2* **2001**, 2355.
(7) Glukhovtsev, M. N.; Bach, R. D.; Nagel, C. J. *J. Phys. Chem. A* **1998**, *102*, 3438.
(8) Patterson, E. V.; Cramer, C. J. *J. Phys. Org. Chem.* **1998**, *11*, 232.
(9) Michalkova, A.; Martinez, J.; Zhikol, O. A.; Gorb, L.; Shishkin, O. V.; Leszczynska, D.; Leszczynski, J. *J. Phys. Chem. B* **2006**, *110*, 21175.
(10) Wagner, G. W.; Bartram, P. W. *J. Mol. Catal. A. Chem.* **1996**, *111*, 175; *J. Mol. Catal. A. Chem.* **1999**, *144*, 419.
(11) Jang, B. W. L.; Spivey, J. J. *Catal. Today* **2000**, *55*, 3.
(12) Frisch, M. J.; Trucks, G. W.; Schlegel, H. B.; Scuseria, G. E.; Robb, M. A.; Cheeseman, J. R.; Montgomery, J. A., Jr.; Vreven, T.; Kudin, K. N.; Burant, J. C.; Millam, J. M.; Iyengar, S. S.; Tomasi, J.; Barone, V.; Mennucci, B.; Cossi, M.; Scalmani, G.; Rega, N.; Petersson, G. A.; Nakatsuji, H.; Hada, M.; Ehara, M.; Toyota, K.; Fukuda, R.; Hasegawa, J.; Ishida, M.; Nakajima, T.; Honda, Y.; Kitao, O.; Nakai, H.; Klene, M.; Li, X.; Knox, J. E.; Hratchian, H. P.; Cross, J. B.; Bakken, V.; Adamo, C.; Jaramillo, J.; Gomperts, R.; Stratmann, R. E.; Yazyev, O.; Austin, A. J.; Cammi, R.; Pomelli, C.; Ochterski, J. W.; Ayala, P. Y.; Morokuma, K.; Voth, G. A.; Salvador, P.; Dannenberg, J. J.; Zakrzewski, V. G.; Dapprich, S.; Daniels, A. D.; Strain, M. C.; Farkas, O.; Malick, D. K.; Rabuck, A. D.; Raghavachari, K.; Foresman, J. B.; Ortiz, J. V.; Cui, Q.; Baboul, A. G.; Clifford, S.; Cioslowski, J.; Stefanov, B. B.; Liu, G.; Liashenko, A.; Piskorz, P.; Komaromi, I.; Martin, R. L.; Fox, D. J.; Keith, T.; Al-Laham, M. A.; Peng, C. Y.; Nanayakkara, A.; Challacombe, M.; Gill, P. M. W.; Johnson, B.; Chen, W.; Wong, M. W.; Gonzalez, C.; Pople, J. A. *Gaussian 03*, revision C.02; Gaussian, Inc.: Wallingford, CT, 2004.
(13) Suenram, R. D.; Lovas, F. J.; Plusquellic, D. F.; Lesarri, A.; Kawashima, Y.; Jensen, J. O.; Samuels, A. C. *J. Mol. Spectrosc.* **2002**, *211*, 110.
(14) Vishnyakov, A.; Neimark, A. V. *J. Phys. Chem. A* **2004**, *108*, 1435.
(15) Florián, J.; Štrajbl, M.; Warshel, A. *J. Am. Chem. Soc.* **1998**, *120*, 7959.
(16) Ault, B. S.; Balboa, A.; Tevault, D.; Hurley, M. *J. Phys. Chem. A* **2004**, *108*, 10094.
(17) Kaczmarek, A.; Gorb, L.; Sadlej, A. J.; Leszczynski, J. *Struct. Chem.* **2004**, *15*, 517.
(18) Walker, A. R. H.; Suenram, R. D.; Samuels, A.; Jensen, J.; Ellzy, M. W.; Lochner, J. M.; Zeroka, D. *J. Mol. Spectrosc.* **2001**, *207*, 77.
(19) Wong, M. W. *Chem. Phys. Lett.* **1996**, *256*, 391.
(20) Andersson, M. P.; Uvdal, P. *J. Phys. Chem. A* **2005**, *109*, 2937.
(21) Scott, A. P.; Radom, L. *J. Phys. Chem.* **1996**, *100*, 16502.
(22) Irikura, K. K.; Johnson, R. D., III; Kacker, R. N. *J. Phys. Chem. A* **2005**, *109*, 8430.
(23) Moravie, R. M.; Froment, F.; Corset, J. *Spectrochim. Acta.* **1989**, *45A*, 1015.
(24) Bertilsson, L.; Engquist, I.; Liedberg, B. *J. Phys. Chem. B* **1997**, *101*, 6021.
(25) Rockley, N. L.; Rockley, M. G. *Appl. Spectrosc.* **1987**, *41*, 471.
(26) Rusu, C. N.; Yates, J. T., Jr. *J. Phys. Chem. B* **2000**, *104*, 12292.
(27) Snyder, R. G.; Hsu, S. L.; Krimm, S. *Spectrochim. Acta.* **1978**, *34A*, 395; Snyder, R. G.; Schachtschneider, J. H. *Spectrochim. Acta.* **1963**, *19*, 85.
(28) Bermudez, V. M. *J. Phys. Chem. B* **2005**, *109*, 9970.
(29) Kuiper, A. E. T.; van Bokhoven, J. J. G. M.; Medema, J. *J. Catal.* **1976**, *43*, 154.
(30) Green, J. H. S. *Trans. Faraday Soc.* **1963**, *59*, 1559.
(31) McGarvey, D. J.; Stuff, J. R.; Williams, B. R.; Durst, H. D. *Spectrosc. Lett.* **2000**, *33*, 795; (Erratum) *Spectrosc. Lett.* **2001**, *34*, 253.
(32) Pinto, H. P.; Nieminen, R. M.; Elliott, S. D. *Phys. Rev. B* **2004**, *70*, 125402.
(33) Pinto, H. P.; Elliott, S. D. *MRS Symp. Proc.* **2003**, *786*, E5.21.
(34) Figures 3 and 4 were constructed using the VENUS set of programs provided at http://homepage.mac.com/fujioizumi/visualization/VENUS.html by R.A. Dilanian and F. Izumi.
(35) Wolverton, C.; Hass, K. C. *Phys. Rev. B* **2000**, *63*, 024102.
(36) Gutiérrez, G.; Taga, A.; Johansson, B. *Phys. Rev. B* **2001**, *65*, 012101.
(37) Krokidis, X.; Raybaud, P.; Gobichon, A.-E.; Rebours, B.; Euzen, P.; Toulhoat, H. *J. Phys. Chem. B* **2001**, *105*, 5121.
(38) Digne, M.; Sautet, P.; Raybaud, P.; Euzen, P.; Toulhoat, H. *J. Catal.* **2004**, *226*, 54; *J. Catal.* **2002**, *211*, 1.
(39) Cai, S.-H.; Rashkeev, S. N.; Pantelides, S. T.; Sohlberg, K. *Phys. Rev. B* **2003**, *67*, 224104.
(40) Paglia, G.; Rohl, A. L.; Buckley, C. E.; Gale, J. D. *Phys. Rev. B* **2005**, *71*, 224115; Paglia, G.; Božin, E. S.; Billinge, S. J. L. *Chem. Mater.* **2006**, *18*, 3242.
(41) Menéndez-Proupin, E.; Gutiérrez, G. *Phys. Rev. B* **2005**, *72*, 035116.
(42) Sun, M.; Nelson, A. E.; Adjaye, J. *J. Phys. Chem. B* **2006**, *110*, 2310.
(43) Digne, M.; Raybaud, P.; Sautet, P.; Rebours, B.; Toulhoat, H. *J. Phys. Chem. B* **2006**, *110*, 20719. Paglia, G.; Buckley, C. E.; Rohl, A. L. *J. Phys. Chem. B* **2006**, *110*, 20721. Nelson, A. E.; Sun, M.; Adjaye, J. *J. Phys. Chem. B* **2006**, *110*, 20724.
(44) Lattice planes are labeled in refs 32 and 33 according to the spinel lattice from which the γ-Al_2O_3 structure is derived. This is standard practice in the literature on γ-Al_2O_3 and will employed here. The (111), (001), and (110) spinel planes correspond, respectively, to the (010), (101), and (001) planes of the conventional (i.e., crystallographic or non-primitive) γ-Al_2O_3 unit cell in Figure 3.
(45) Knözinger, H.; Ratnasamy, P. *Catal. Rev. Sci. Eng.* **1978**, *17*, 31.
(46) Dyan, A.; Cenedese, P.; Dubot, P. *J. Phys. Chem. B* **2006**, *110*, 10041.
(47) Jug, K.; Bredow, T. *J. Comput. Chem.* **2004**, *25*, 1551.
(48) Lü, X.; Xu, X.; Wang, N.; Zhang, Q.; Ehara, M.; Nakatsuji, H. *Chem. Phys. Lett.* **1998**, *291*, 445.
(49) Wittbrodt, J. M.; Hase, W. L.; Schlegel, H. B. *J. Phys. Chem. B* **1998**, *102*, 6539.
(50) Hass, K. C.; Schneider, W. F.; Curioni, A.; Andreoni, W. *J. Phys. Chem. B* **2000**, *104*, 5527.
(51) Herschend, B.; Baudin, M.; Hermansson, K. *Surf. Sci.* **2005**, *599*, 173.
(52) Pacchioni, G.; Ferrari, A. M.; Márquez, A. M.; Illas, F. *J. Comput. Chem.* **1997**, *18*, 617. Ferrari, A. M.; Pacchioni, G. *Int. J. Quant. Chem.* **1996**, *58*, 241.
(53) Catlow, C. R. A.; French, S. A.; Sokol, A. A.; Thomas, J. M. *Phil. Trans. R. Soc. A.* **2005**, *363*, 913. Sokol, A. A.; Bromley, S. T.; French, S. A.; Catlow, C. R. A.; Sherwood, P. *Int. J. Quant. Chem.* **2004**, *99*, 695.
(54) Injan, N.; Pannorad, N.; Probst, M.; Limtrakul, J. *Int. J. Quantum. Chem.* **2005**, *105*, 898. Dungsrikaew, V.; Limtrakul, J.; Hermansson, K.; Probst, M. *Int. J. Quantum Chem.* **2004**, *96*, 17.
(55) Batista, E. R.; Friesner, R. A. *J. Phys. Chem. B* **2002**, *106*, 8136.
(56) Stefanovich, E. V.; Truong, T. N. *J. Phys. Chem. B* **1998**, *102*, 3018.
(57) Nasluzov, V. A.; Rivanenkov, V. V.; Gordienko, A. B.; Neyman, K. M.; Birkenheuer, U.; Rösch, N. *J. Chem. Phys.* **2001**, *115*, 8157. Nasluzov, V. A.; Ivanova, E. A.; Shor, A. M.; Vayssilov, G. N.; Birkenheuer, U.; Rösch, N. *J. Phys. Chem. B* **2003**, *107*, 2228.

(58) Yudanov, I. V.; Nasluzov, V. A.; Neyman, K. M.; Rösch, N. *Int. J. Quant. Chem.* **1997**, *65*, 975.
(59) Mitchell, M. B.; Sheinker, V. N.; Mintz, E. A. *J. Phys. Chem. B.* **1997**, *101*, 11192. Sheinker, V. N.; Mitchell, M. B. *Chem. Mater.* **2002**, *14*, 1257.
(60) Aurian-Blajeni, B.; Boucher, M. M. *Langmuir* **1989**, *5*, 170.
(61) Templeton, M. K.; Weinberg, W. H. *J. Am. Chem. Soc.* **1985**, *107*, 97; *J. Am. Chem. Soc.* **1985**, *107*, 774.
(62) Davies, P. R.; Newton, N. G. *Appl. Surf. Sci.* **2001**, *181*, 296.
(63) Simon, S.; Duran, M.; Dannenberg, J. J. *J. Chem. Phys.* **1996**, *105*, 11024.
(64) Moskaleva, L. V.; Nasluzov, V. A.; Chen, Z.-X.; Rösch, N. *Phys. Chem. Chem. Phys.* **2004**, *6*, 4505.
(65) Casarin, M.; Falcomer, D.; Glisenti, A.; Vittadini, A. *Inorg. Chem.* **2003**, *42*, 436. Casarin, M.; Maccato, C.; Vittadini, A. *Inorg. Chem.* **2000**, *39*, 5232.
(66) Wagner, G. W.; Procell, L. R.; O'Connor, R. J.; Munavalli, S.; Carnes, C. L.; Kapoor, P. N.; Klabunde, K. J. *J. Am. Chem. Soc.* **2001**, *123*, 1636.
(67) van Bokhoven, J. J. G. M.; Kuiper, A. E. T.; Medema, J. *J. Catal.* **1976**, *43*, 168; *J. Catal.* **1976**, *43*, 181.
(68) Cioslowski, J. *J. Am. Chem. Soc.* **1989**, *111*, 8333.